Correlations in TLS point clouds: Should we care about them?

Gabriel KEREKES[1,*], and **Volker SCHWIEGER**[1]

[1] *Institute of Engineering Geodesy – University of Stuttgart, Stuttgart, Germany, (gabriel.kerekes@iigs.uni-stuttgart.de)*

[*] *corresponding author*

Abstract

High-end Terrestrial Laser Scanners (TLSs) are used for many applications that require precise geometry of the captured object. Dimensions are frequently extracted directly from the point cloud or from estimated primitives. However, the uncertainty information attributed to each point and correlations between points are often neglected. Generally, TLS observations may be highly correlated for reasons such as similarities in the surface properties, instrument optical-mechanical misalignments, overlap of laser footprints, or similarities in the measurement environment. The current contribution demonstrates the relevance of correlations in tasks usually performed directly with the point cloud, such as distance measurements between two points, target segmentation based on point clouds (e.g., spheres), and registration. Tests were conducted using the variance-covariance propagation law and elementary error theory for simple distance measurements between highly correlated points (e.g., $\rho=0.8$). Firstly, simulation results are used to show that precision estimations for measured distances are up to 55% better with correlations than without. The same analysis is done with real data, and an improvement of the precision estimate of 20% was reached; however, degradation is also possible if negative correlations occur. Additionally, the impact of correlations on the sphere-based registration between two TLS station points is shown. The spheres were segmented, and center coordinates were estimated using different versions of a stochastic model. Finally, they were used in the registration. Conclusions about correlations in TLS point clouds are drawn based on these tasks encountered in almost all TLS applications.

Keywords: Uncertainty propagation, statistical testing, quality control, registration, primitive estimation

Received: 2nd December 2024. Revised: 16th February 2025. Accepted: 28th February 2025.

1 Introduction

Point clouds acquired with Terrestrial Laser Scanners (TLSs) have become ubiquitous for many surveying tasks. Laser scanners have reached a development state that allows high acquisition rates, such as more than 2 million points per second with millimeter accuracy (Wieser et al., 2019). In most cases, the uncertainty information of the point cloud is not asserted by the user because the topic is complex and depends on factors such as the instruments' technical specifications, the scanner's position relative to the scanned object, the object's surface radiometric properties, and in some cases, the local environment conditions (cf. Kerekes, 2023). However, in tasks that require accurate geometric dimensioning of the captured object, questions about the uncertainty of the measurements are usually the first that the beneficiaries pose. Moreover, if the uncertainty information is used for geometric segmentation, it may influence the results of the respective segmented primitive. Another common task for TLS point clouds is the registration of multiple station points. Whether target-based or feature-based, computing the position of consecutive TLS station points translates into computing a 3D transformation. To the author's best knowledge, uncertainty information about the targets and features is not used in commercially available software for the transformation, but only in science. The current contribution aims to analyze the effects of variance-covariance propagation, with focus on correlations in the following TLS applications:

1. Distance measurements between two points
2. Estimation of geometric primitives
3. Target-based registration between two station points

It can be demonstrated that in each case, the role of correlations is mostly underestimated, and efforts should be made to determine them despite the current technical limitations for huge point clouds.

2 Sources of TLS correlations

2.1 Literature review

Although progress has been made in defining a stochastic model for TLS (cf. Gordon, 2008; Wujanz et al., 2017; Kerekes, 2023; Jost, 2023), research is still needed to fully describe the uncertainty budget of point clouds and the effects of these uncertainties on the outcomes. Furthermore, if measurements are influenced by the same sources, such as similar surface properties, or emerge from the same sources (e.g., laser scanner), it is assumed that they are correlated with each other. The topic is not new for geodetic measurements (cf. Gotthardt, 1960; Heunecke, 2004) but has not been fully studied specifically for TLS measurements. Only a relatively reduced number of publications deal with TLS correlations up to date (Koch, 2008; Alkhatib et al., 2009; Lichti, 2010; Kauker et al., 2017; Jurek et al., 2017; Kermarrec & Lösler, 2020; Schmitz et al., 2021; Kerekes et al., 2022), most of which are for complex tasks encountered in the scientific community. From the above-mentioned publications, it can be concluded that correlations are derived from the following main sources:

- instrument optical-mechanical misalignments;
- similarities in the surface properties;
- overlapping of laser footprints;
- similarities in the measurement environment.

Independent of how the correlations are computed, whether empirically or synthetically, the complete stochastic model can be described in the general form of a variance-covariance matrix (eq. 1).

$$\boldsymbol{\Sigma}_{ll_{xyz}} = \begin{bmatrix} \sigma_{x_1}^2 & \sigma_{x_1y_1} & \sigma_{x_1z_1} & \sigma_{x_1x_2} & \sigma_{x_1y_2} & \sigma_{x_1z_2} & \cdots \\ & \sigma_{y_1}^2 & \sigma_{y_1z_1} & \sigma_{y_1x_2} & \sigma_{y_1y_2} & \sigma_{y_1z_2} & \cdots \\ & & \sigma_{z_1}^2 & \sigma_{z_1x_2} & \sigma_{z_1y_2} & \sigma_{z_1z_2} & \cdots \\ & & & \sigma_{x_2}^2 & \sigma_{x_1y_2} & \sigma_{x_2z_2} & \cdots \\ & & & & \sigma_{y_2}^2 & \sigma_{y_2z_2} & \cdots \\ & & & & & \sigma_{z_2}^2 & \cdots \\ & & & & & & \ddots \end{bmatrix} \quad (1)$$

2.2 The origin of correlations in EEM

In the current paper, correlations are computed from fully populated variance-covariance matrices (VCMs) that are either generated based on the variance-covariance propagation law (VCPL) and elementary error model (EEM), as described in Kerekes (2023) or generated based on given correlation coefficients between pairs of coordinates of two points. Only random deviations are addressed here, and the assumption is that they are normally distributed; therefore, applying the VCPL is eligible. Note that in this contribution, the term correlations may refer to mathematical correlations resulting from the functional relation between observations or to physical correlations resulting from external influences (e.g., same surface properties). The origin of correlations in this case are, on one side, the instrumental errors in the functional correlating group and the errors for the object surface properties. Other types of errors, such as non-correlating errors, do not lead to correlations and the atmospheric influences are neglected for the laboratory conditions. Numeric values in the VCMs generated by the EEM are values obtained empirically and verified in the authors' previous publications. It is strongly recommended to consult these publications for an in depth understanding of the EEM.

The novelty in the current paper compared to previous work (Kerekes, 2023; Kerekes & Schwieger, 2024) is that the errors for object surface properties are now modeled as functional correlating, and the VCM for reflectivity is not generalized for a single surface (e.g., arch dam or façade plate).

A detailed explanation is given for obtaining $\boldsymbol{\Sigma}_{\gamma\gamma-\mathrm{ref}}$, the VCM due to object surface properties. The main diagonal of $\boldsymbol{\Sigma}_{\gamma\gamma-\mathrm{ref}}$ is available based on the polynomial function that gives the standard deviation of each measured range as a function of reflectance and range (cf. Kerekes & Schwieger, 2024, tab. 3). In order to describe the similarities, and implicitly the correlations, between the effects on the ranges, an additional correlation matrix **R** is necessary. Note that a correlation matrix is independent of the absolute values of the VCM from which it has been derived. In the current case, the challenge is to firstly define a correlation matrix and afterwards use the correlations to obtain the covariances in $\boldsymbol{\Sigma}_{\gamma\gamma-\mathrm{ref}}$, since the main diagonal is already available. The workflow is presented in figure 1.

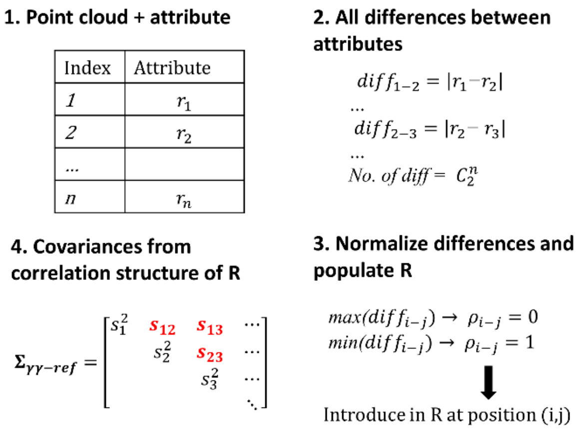

Figure 1. Workflow for deriving correlations

Given the attribute reflectance for all n points (Fig. 1-1), differences between all pairs of attributes can be computed (Fig. 1-2). This results in a number C_2^n of unique pairs of differences for the respective attribute. In step three (Fig. 1-3), the values are normalized according to the principle highest difference leads to lowest correlation $\rho = 0$ and lowest difference means highest similarity and thereafter highest correlation $\rho = 1$. Values in between are interpolated. In the case of reflectance, values can theoretically vary from 0% to 100%. The largest difference is 100% in this case, and the smallest is 0% (e.g., two points have the same values for reflectance). The same approach can be applied for other influencing factors, such as the measured ranges in this case. For each of the computed differences, the point index from step 1 (Fig. 1-1) is known, therefore the correlation coefficients for each pair $i - j$ is introduced in $\mathbf{R}$ at position (i, j). If several sources of correlation need to be combined, like in the current case (e.g. reflectance and range), the needed correlation matrix is obtained as the Hadamard product (element-wise product) $\mathbf{R} = \boldsymbol{R_1} \odot \boldsymbol{R_2}$. Finally, using the main diagonal of $\boldsymbol{\Sigma}_{\gamma\gamma-\text{ref}}$ together with correlations coefficients from $\mathbf{R}$, the covariances in $\boldsymbol{\Sigma}_{\gamma\gamma-\text{ref}}$ are computed (Fig. 1-4).
Although simple, the validity of this approach is shown later by introducing the resulting correlations in the sphere estimation.

3 Relevance of correlations in common tasks with point clouds

3.1 Distance between two points

Tools for measuring distances directly between two points in the point cloud are available in most of the software that deal with point clouds. In these software it is possible to obtain dimensions between manually selected points. However, none of them indicate the precision of the respective distance measurements. This is possible only if a stochastic model of the respective point cloud is available. Even if the user propagates the uncertainty as given by the manufacturer (cf. Lipkowski & Mettenleiter, 2019) and defines a simplistic stochastic model, the correlations between the points are not considered. The examples presented here highlight the differences in the uncertainty estimations for simple Euclidian distances D_{ij} (eq. not given here) between pairs of points, with and without correlations defined at different levels. Using the VCPL on the equation for D_{ij} results in a precision estimate of the respective distance (eq. 2). The differences occur based on how the matrix $\boldsymbol{\Sigma}_{\boldsymbol{ll}_{xyz}}$ is populated (diagonal matrix or fully populated matrix). The matrix $\boldsymbol{F}$ is the Jacobian matrix for the functional model of D_{ij}.

$$\sigma_{D_{ij}} = \sqrt{\boldsymbol{F} \cdot \boldsymbol{\Sigma}_{\boldsymbol{ll}_{xyz}} \cdot \boldsymbol{F}^T} \qquad (2)$$

According to the nature of TLS measurements, it is impossible to cover all the scenarios encountered in reality and generalize the outcomes for uncertainty propagation. The numeric values in $\boldsymbol{F}$ strongly depend on the position of the chosen points and the definition of the 3D coordinate system.

To exemplify the impact of correlations in simple distance measurements, a point cloud of a room was captured using static laser scanning with the Leica HDS7000 (Leica Geosystems AG, 2011). The scanning resolution was set to “high”, corresponding to 40 mgon angular increments in both horizontal and vertical directions. This scanner was used because the stochastic model was studied intensively in recent years, and the authors have empirical values for the different error groups of the EEM. Any other point cloud could have been used to extract points in the simulation and real data case.

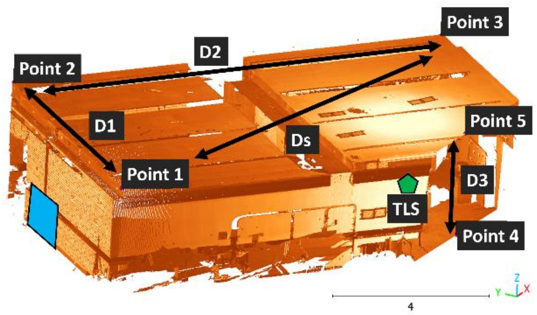

Figure 2. Example point cloud and examined distances

The five points are typical points that a user would choose for the room's dimensions (Fig. 2).
Distances D1 between points 1 – 2 is the room's width, D2 between points 2 – 3 is the room's length, and D3 between points 4 – 5 is the room's height.
First, different correlation coefficient values are simulated for the coordinates of points 1 to 5. The standard deviations of the point's coordinates are all set to an equal level of $\sigma_{x_i} = \sigma_{y_i} = \sigma_{z_i} = 5\ mm$. Afterward, the covariances between different pairs of coordinates (called cases in Table 1) are computed based on the simulated level of correlation ρ, also known as the Pearson correlation coefficient. The levels are chosen with a discretization of 0.2, and the combinations are xyz - all coordinates correlated, xy – only plane coordinates are correlated, and zz – only height coordinates are correlated. Other combinations are also possible, but only these are presented due to limited space.

Table 1. Differences in precision estimates for distances with simulated correlation coefficients

Case	ρ	σ_{D1} [mm] no corr	σ_{D1} [mm] corr	Δ [%]	σ_{D2} [mm] corr	Δ [%]	σ_{D3} [mm] corr	Δ [%]
xyz	0.8		3.2	55%	3.2	55%	3.2	55%
	0.6		4.5	37%	4.5	37%	4.5	37%
	0.4		5.5	23%	5.5	23%	5.5	23%
	0.2		6.3	11%	6.3	11%	6.3	11%
xy	0.8		3.2	55%	3.2	55%	7.0	1%
	0.6	7.1	4.5	37%	4.5	37%	7.0	1%
	0.4		5.5	23%	5.5	23%	7.1	0%
	0.2		6.3	11%	6.3	11%	7.1	0%
zz	0.8		7.1	0%	7.1	0%	3.2	55%
	0.6						4.5	37%
	0.4						5.5	23%
	0.2						6.3	11%

Only the results for the standard deviations according to eq. 2 are shown here. If no correlations are considered, the standard deviations for all three distances remain the same, 7.1 mm. For all other cases with correlations, the numeric values are given in the column "corr," besides the improvement in % relative to the "no corr" case. For all cases, if the coordinates used for D1, D2 and D3, are functionally dependent ($\rho = 1$), eq. 2 yields 0; therefore, this case is not studied. If the correlation level decreases by only 0.2, the resulting standard deviation is 55% smaller for all distances in the case xyz. Afterwards, it decreases proportionally.
In the case of xy (only plane coordinates), differences between the no correlations and correlations values are seen only for D1 and D2. This is due to their position in space, mainly in the xy plane. For D3, almost no difference (1% or 0%) is seen, a fact that is expected according to the functional model for points with almost identical xy coordinates. The last case, zz, shows what should be expected if only the point's heights are correlated. The variances of distances that are approximately on the same plane (D1 and D2) do not change if only their z coordinates are correlated. However, in D3, the room height shows changes between both scenarios. The highest correlation level leads to a 55% smaller standard deviation, and the lowest level of 0.2 still improves the value with 11%. A similar study was done for GNSS measurements by Kermarrec & Schön (2017).

Table 2. Differences in precision estimates for distances with EEM correlation coefficients

Case	ρ	no corr	corr	Δ [%]
		σ_{D1}(1-2) [mm]		
xx	0.44			
yy	0.40	1.487	1.193	20%
zz	0.35			
		σ_{D2} (2-3) [mm]		
xx	-0.25			
yy	0.21	1.400	1.741	-24%
zz	0.37			
		σ_{D3} (4-5) [mm]		
xx	0.19			
yy	-0.02	0.920	0.928	-1%
zz	0.02			
		σ_{Ds} (1-3) [mm]		
xx	-0.33			
yy	-0.01	1.199	1.388	-16%
zz	0.37			

Up to now, this is only a theoretical case. In order to verify the resulting values with real variances and covariances, the EEM and VCPL were used to establish a synthetic variance-covariance matrix (SVCM) for the same five points, and a similar analysis was performed. This time, the correlation coefficients are extracted from the resulting matrix, and the differences are presented in Table 2. Note that the used values for variances and covariances in the EEM are based on empirically verified past studies (e.g., Raschhofer et al., 2021; Kerekes & Schwieger, 2024). In Raschhofer et al., (2021), the non-correlating errors of the Leica HDS7000 were studied using reference B-Spline test objects and values for the angular measurement noise and range noise were empirically obtained. In the same paper, the role of further instrumental errors in the functional correlating group was explained. In Kerekes & Schwieger (2024), an approach was described for obtaining the standard deviations for distance measurements based on a manufacturer-defined function according to the reflectance of the scanned surface and distances. The reflectance values of the scanned room presented in figure 2 are retrieved from another scan using the calibrated reflectance measured with a Riegl VZ2000 scanner. Opposed to how correlations were defined in the previous paper, in the current one, they are obtained using the novelty presented in section 2.

The variances and covariances strongly depend on the position of the five points relative to the scanner. On one side, some of the EEM error groups have a proportional effect on the resulting variances (e.g., non-correlating group), whereas, for others, the correlation level depends on their position (e.g., above the scanner horizon) and the object surface properties (e.g., high vs. low reflectance). Although the absolute value of the standard deviations is low in these cases (under 2 mm), the reader should focus on the relative change when correlations are considered.

For D1, an improvement of the standard deviation of 20% is seen, and only positive correlation coefficients exist between the coordinates. This agrees with the simulated case for a correlation level of around 0.4. An interesting finding is realized for D2. Due to a negative correlation coefficient in the x direction, the case with correlations is 24% worse than the case without correlations. This phenomenon necessitated further inspection; therefore, a supplementary distance Ds situated in the same plane (ceiling) with D2 was considered. Also in this case, negative correlations coefficients were obtained in the x plane. A decay of the precision estimate with 16% can be seen. These effects were analyzed by separating the contributing elementary errors in each group (non- correlating, functional correlating instrumental errors and, functional correlating group with object surface properties). Single VCM were computed and the correlation level were analyzed separately. For D2 and Ds the correlations in the x plane with functional correlating instrumental errors only are 0.54 and 0.03. Interestingly for the same combinations, strong negative correlations in the y plane are seen (-0.64 and -0.96) and strong positive ones in the z plane (0.97 and 0.98). Adding the non-correlating errors (only main diagonal), reduces the correlations in the x plane to 0.04 and 0, practically making the points uncorrelated. Finally, with the object properties group they become negative and reach the values shown in table 2. This is traced back to the influences of the scanning geometry (angle of incidence and measured range) of these points.

For the room height, D3, almost no difference is seen besides a slight change in µm level, which may be considered insignificant. This also corresponds to the simulated scenario where no change is observed if only plane coordinates (here x) are correlated.

In addition to these five points, another four were chosen. They are all scanned points on a 1x1 m reference reflectance plate (SphereOptics) with different reflectance properties that are very well known (e.g., 20%, 50%, 80%). They are depicted in numbers 6 to 9 to differentiate them from the previous ones. The plate's position relative to the scanner is seen in Figure 2 and depicted by the blue square. The position of the four points is shown in Figure 3.

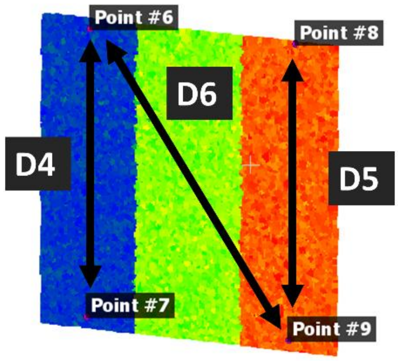

Figure 3. Points on SphereOptics reflectance plate

Points 6 and 7 show 20% reflectance, and 8 and 9 are on the part with 80%. From the point of view of surface reflectance, D4 and D5 are from points that are relatively highly correlated with each other, whereas D6 is not correlated based on reflectance.

Table 3. Differences in precision estimates for distances on reflectance plate

Case	ρ	σ_{D4} (6-7) [mm]		
		no corr	corr	Δ [%]
xx	0.53	0.787	0.624	21%
yy	0.63			
zz	0.36			
		σ_{D5} (8-9) [mm]		
xx	0.30	0.785	0.633	19%
yy	0.40			
zz	0.34			
		σ_{D6} (6-9) [mm]		
xx	0.08	0.837	0.638	19%
yy	0.04			
zz	0.33			

In all three cases (Table 3), a difference of around 20% is observed, showing an improvement of the distance computed uncertainty with correlations. Although the effects are less obvious than in the previous case, some coordinates are more correlated. The height of all three cases remains at a

constant level of around 0.3. Note that the plate was placed vertically against the wall. Therefore, the standard deviation obtained for this level of correlation is in concordance with the one obtained for D3 in the simulated scenario, where points are at different heights. Moreover, as in the simulated case, the correlations in the plane coordinates x and y do not contribute to the change of the standard deviation with correlations, even if they are very low, 0.04 (for D6) or relatively high 0.63 (for D5).
Overall, it can be seen that taking correlations into consideration is important for tasks such as distance measurements extracted from the point cloud, and a change of ca. 20% (not only improvements) should be expected.

3.2 Sphere estimation

TLS targets in spherical forms are used for georeferencing or registration in many practical applications. The coordinates of the sphere center are determined after an adjustment, a procedure that mostly happens directly in the TLS proprietary software. As an output, the user obtains the sphere's center coordinates but does not always receive detailed information about the coordinate's precision for each coordinate. For example, in Leica Cyclone (v. 2023.1.0), the user can only evaluate the fit quality by a few global indicators, the mean error, and a standard deviation. In other commercially available software, this information is likewise sparse or inexistent. This may be an issue if the sphere center coordinates are needed for deformation analysis (Yang et al., 2021), where the stochastic properties of center coordinates are used for statistically based decisions.
The user may also use the points on the sphere and conduct an adjustment independent of the TLS software to obtain a measure for uncertainty estimation. However, usually, the high number of points on the sphere leads to results that are, in most cases, too optimistic (cf. Yang et al., 2021). In any case, results will be treated as unrealistic. This phenomenon is due to the inconsideration of an appropriate stochastic model in the adjustment.
In order to prove the effects of including correlations in the estimation of a sphere's center coordinates, examples are given with scanned TLS spheres in laboratory conditions. These are 14 cm diameter TLS spheres that will be used later for the registration of two TLS point clouds. The spheres were scanned from distances varying from 3.2 m to 9.4 m. Each sphere was manually segmented, and systematic effects caused by mixed pixels were manually deleted. In some cases, an interesting phenomenon was observed for points where the TLS intensity was maximum in the middle of the sphere surface. Distances were falsified, and the points were obviously outside of the sphere's surface. These points are likewise treated as outliers and eliminated from the sphere adjustment. All spheres were scanned from two TLS station points.

Figure 4. Position of TLS spheres and station points

The relative position is depicted in a point cloud in Fig. 4. For all spheres, the reflectance information is retrieved from a point cloud captured with the Riegl VZ2000. The conversion from dB to % is done as in Kerekes & Schwieger (2024).
Niemeier (2008) gives the theoretical background for the Gauß-Helmert-Model (GHM) used to estimate the center coordinates of points observed on a circle, whilst the same model is presented for a sphere in Jäger et al. (2005).
The focus is set on the role of correlations from the SVCM in the GHM adjustment. The analysis is done with two different versions of the same SVCM. The difference is as follows:

- $\Sigma_{ll} = D$ is the main diagonal of the SVCM;
- $\Sigma_{ll} = SVCM$ is the fully populated SVCM.

Comparing these stochastic models shows the influence of the correlations on the adjusted coordinates of the sphere center points and their corresponding uncertainties.
The SVCM used in this adjustment is established with values from past experiences, as shown in section 3.1. together with the new approach for defining correlations mentioned in section 2.2.

In Table 4, the results are shown for the standard deviations of the estimated center coordinates, and finally, the square root $\hat{s}_0$ of the a posteriori variance factor $\hat{s}_0^2$ as a global indicator for the adjustment. The assumed a priori variance factor of $\sigma_0^2 = 1$ (dimensionless) is used in common cases.
The first important finding is that the difference in the estimated values of the sphere center coordinates in all cases is not noticeable (µm level) and therefore not shown here.

Table 4. Sphere estimation results

Target in PC	Stochastic model	$s_x[mm]$	$s_y[mm]$	$s_z[mm]$	$\hat{s}_0$	Points on sphere	Distance scanner [m]
T1_K2	$\Sigma_{ll} = D$	0.065	0.129	0.046	0.56	374	9.440
	$\Sigma_{ll} = SVCM$	0.108	0.143	0.102	0.66		
T2_K2	$\Sigma_{ll} = D$	0.052	0.020	0.017	0.71	1503	4.865
	$\Sigma_{ll} = SVCM$	0.155	0.147	0.146	**1.09**		
T3_K2	$\Sigma_{ll} = D$	0.033	0.011	0.011	0.67	2808	3.245
	$\Sigma_{ll} = SVCM$	0.161	0.157	0.157	1.43		
T1_K3	$\Sigma_{ll} = D$	0.013	0.024	0.011	0.50	2448	3.981
	$\Sigma_{ll} = SVCM$	0.125	0.127	0.126	**0.97**		
T2_K3	$\Sigma_{ll} = D$	0.150	0.127	0.071	0.89	423	8.745
	$\Sigma_{ll} = SVCM$	0.211	0.200	0.178	**1.25**		
T3_K3	$\Sigma_{ll} = D$	0.018	0.051	0.018	0.67	1395	4.923
	$\Sigma_{ll} = SVCM$	0.163	0.175	0.165	**1.07**		

The standard deviations are in the sub-mm level. Using the SVCM main diagonal compared to the fully populated SVCM leads in all cases to smaller standard deviations. If correlations are considered, there are cases where they are 10 times larger (e.g., T1_K3, or in some cases, the differences are relatively small (e.g., T1_K2 in y direction) of a few µm. Even if they may be irrelevant for some TLS tasks, these kinds of changes make a difference in the decisions of deformation analysis, as demonstrated by Yang et al. (2021).

Next, the more relevant parameter $\hat{s}_0$ for the complete adjustment, is analyzed. A change is observed in all estimations. In practice, the closer it approaches the value 1 (a-priori level), it can be affirmed that the functional model is valid, the stochastic model is appropriate, and no outliers exist (cf. Niemeier, 2008). If the level of variance and covariances are chosen too optimistic, then $\hat{s}_0 > 1$, and if they are too pessimistic $\hat{s}_0 < 1$ (Heunecke et al., 2013). Acceptance intervals for the global test generally considered in geodesy for adjustments are between [0.7 … 1.3] (cf. Möser et al., 2012), although the upper and lower acceptance boundaries can be rigorously obtained from the critical values of the F-distribution function or normalized χ^2 distribution based on the degrees of freedom (cf. Jäger et al., 2006; Niemeier, 2008).

By using the identity matrix $\boldsymbol{P} = \boldsymbol{I}$ (not shown in the table), $\hat{s}_0$ does not approach the value of 1, and in all cases, it is a too pessimistic approach. In cases depicted by $\Sigma_{ll} = D$ for brevity, observations are weighted according to the diagonal SVCM, which, in some isolated cases, is also an appropriate stochastic model (e.g., T2_K3). However, using only the main diagonal is a slightly too pessimistic choice for sphere estimation.

Finally, the fully populated matrix $\Sigma_{ll} = SVCM$ offers the overall best results for four out of six spheres, for which the global test is fulfilled. Noteworthy is that for the second station point (K3), the test is passed for all three spheres. Whereas, for K2, the two exceptions, T1_K2 and T3_K2, do not fulfill the test. One value is slightly below, and one is slightly above the acceptance interval. Although all outliers were eliminated iteratively based on a simple 2σ rule, $\hat{s}_0$ did not improve. The reasons remain unclear at the moment.

Overall, it can be affirmed that by using the full SVCM, the estimation results are more realistic compared to the other cases and demonstrate that including the spatial correlations is beneficial for sphere estimation. The VCMs for the estimated coordinates (3x3 matrix) are also used for the following analysis in the registration.

3.3 Registration

In the setup used for sphere estimation, the minimum number of three corresponding points is available for each TLS point. To demonstrate the effects of correlations in a 4-parameter transformation, the open-source software Java Applied Geodesy (JAG3D) (Lösler, 2024) was used. Along with the three translations, the rotation around z is estimated. The other two rotation angles are not estimated because the Leica HDS7000 was leveled at each station point.

The coordinates of the sphere's centers were taken directly from Table 4, and the VCM matrixes for the spheres in the two cases (diagonal SVCM, $\Sigma_{ll} = D$ and full SVCM, $\Sigma_{ll} = SVCM$) are introduced in the transformation. Note that correlations in the $\Sigma_{ll} = SVCM$ case are computed with the EEM and applied with the variances derived in section 3.2. Ideally, the correlations should result from a simultaneous multiple-sphere GHM adjustment; however, obtaining this solution poses a technical challenge in handling the point cloud. Additionally, the case with equally weighted coordinates $\Sigma_{ll} = I$ is shown. The estimates for the transformation parameters are shown together with the corresponding uncertainty.

Table 5. Transformation parameters with different versions of the sphere estimation stochastic model

Stochastic model from sphere estimation	Parameter	Estimated value [m] or [gon]	σ [mm] or [mgon]
$\Sigma_{ll} = I$	Tx	-1.7738	3.4
	Ty	5.2608	3.2
	Tz	-0.0136	3.1
	Rot_z	208.17993	35.58
$\Sigma_{ll} = D$	Tx	-1.7786	1.7
	Ty	5.2665	2.1
	Tz	-0.0132	1.0
	Rot_z	208.18051	18.6
$\Sigma_{ll} = SVCM$	Tx	-1.7758	2.0
	Ty	5.2615	2.5
	Tz	-0.0134	3.1
	Rot_z	208.1553	25.3

In each case, the estimated translation values differ in the lower mm level with minor differences. The used experimental setup is not designed to compare the estimated values against a true value of the scanner's position (e.g., pilar with precisely known coordinates). However, this implies exact knowledge of the scanner's local coordinate system origin (not 0,0,0 in the point cloud), which is not trivial to determine. An approach to validate the estimated transformation parameters would be to use a calibration room with reference geometric shapes, such as a sphere for which each scan covers a hemisphere. One could use the points on the reference sphere from each station point and see which version of the registration leads to the best sphere estimation (e.g. by the same approach as in section 3.2). Therefore, judging from how the parameters affect the registrations remains a subject for further research.

If the uncertainty parameters of the transformation parameters are assessed, it can be seen that by using a stochastic model, all values improve compared to equally weighted coordinates $\Sigma_{ll} = I$. Using the diagonal VCM led to the overall lowest level of uncertainty for the translation parameters and rotation angle. If the full VCM with correlations between the sphere's centers are considered, the results are better than those with the unity matrix; however, they are slightly worse than the diagonal matrix. It can be affirmed that both versions of the SVCM (diagonal and fully populated) introduced in the sphere estimation improve the registration uncertainty.

4 Conclusions

This study focused on the role of correlations in different tasks commonly encountered in TLS. It was shown that high correlations have an impact on the uncertainty estimation of distances between two points in the simulated scenario. In a real case, improvements of up to 21% were determined, but a deterioration of 24% was also identified for negatively correlated coordinates.

In most cases, introducing correlations in a GHM adjustment for sphere center coordinates estimation proved beneficial for the estimated six spheres. The global test for the adjustment was used to verify if the derived correlations were realistic.

In a further analysis, the impact of an appropriate stochastic model on the registration of two points was shown. It was seen that using the SVCM defined with the EEM in the sphere estimation reduced the uncertainty of the registered point cloud in both cases with and without correlations. However, the effects of the transformation parameters on the point cloud remain a topic for future research.

References

Alkhatib, H., Neumann, I., & Kutterer, H. (2009). Uncertainty modeling of random and systematic errors by means of Monte Carlo and fuzzy techniques. *Journal of Applied Geodesy*, *3*(2).

Gordon, B. (2008). *Zur Bestimmung von Messunsicherheiten terrestrischer Laserscanner*. PhD Thesis, Technische Universität Darmstadt.

Gotthardt, E. (1960). Zur Ermittlung von Korrelationen. *Zeitschrift Für Vermessungswesen 1960*, *85*(6).

Heunecke, O. (2004). Nochmals über Korrelationen in der Messtechnik. *Festschrift Univ. Prof. H. Pelzer Zur Emeritierung Schriftenreihe Der Fachrichtung Vermessungswesen Der Universität Hannover*, *120*.

Heunecke, O., Kuhlmann, H., Welsch, W., Eichhorn, A., & Neuner, H. (2013). *Auswertung Geodätischer Überwachungsmessungen* (M. Möser, G. Müller, & H. Schlemmer, Eds.; 2nd ed., p. 198). Handbuch Ingenieurgeodäsie, Wichmann.

Jäger, R., Müller, T., Saler, H., & Schwäble, R. (2006). *Klassische und robuste Ausgleichungsverfahren: Ein Leitfaden für*

Ausbildung und Praxis von Geodäten und Geoinformatikern. Herbert Wichmann.

Jost, B. H. (2023). *Strategies for the empirical determination of the stochastic properties of terrestrial laser scans*. PhD Thesis, Rheinische Friedrich-Wilhelms-Universität Bonn.

Jurek, T., Kuhlmann, H., & Holst, C. (2017). Impact of spatial correlations on the surface estimation based on terrestrial laser scanning. *Journal of Applied Geodesy*, *11*(3).

Kauker, S., Harmening, C., Neuner, H., & Schwieger, V. (2017). Modellierung und Auswirkung von Korrelationen bei der Schätzung von Deformationsparametern beim terrestrischen Laserscanning. *Proceedings of 18. International Ingenieurvermessungskurs in Graz*. Herbert Wichmann.

Kerekes, G. (2023). *An Elementary Error Model for Terrestrial Laser Scanning*. PhD Thesis. Universität Stuttgart.

Kerekes, G., Raschhofer, J., Harmening, C., Neuner, H., & Schwieger, V. (2022). Two-epoch TLS deformation analysis of a double curved wooden structure using approximating B-spline surfaces and fully-populated synthetic covariance matrices. *Proceedings of 5th Joint International Symposium on Deformation Monitoring (JISDM), 6-8 April 2022, Valencia, Spain*.

Kerekes, G. & Schwieger, V. (2024). An approach for considering the object surface properties in a TLS stochastic model. *Journal of Applied Geodesy*, *18*(1).

Kermarrec, G., & Lösler, M. (2020). How to account for temporal correlations with a diagonal correlation model in a nonlinear functional model: a plane fitting with simulated and real TLS measurements. *Journal of Geodesy*, *95*(1).

Kermarrec, G., & Schön, S. (2017). Taking correlations into account: a diagonal correlation model. GPS Solutions, 21(4).

Koch, K.-R. (2008). Determining uncertainties of correlated measurements by Monte Carlo simulations applied to laserscanning. *Journal of Applied Geodesy*, 2(3).

Leica Geosystems AG (2011). Datasheet HDS 7000 Laser Scanner. Available from the archives at: https://leica-geosystems.com/

Lichti, D. D. (2010). Terrestrial laser scanner self-calibration: Correlation sources and their mitigation. *ISPRS Journal of Photogrammetry and Remote Sensing*, *65*(1).

Lipkowski, S., & Mettenleiter, M. (2019). Terrestrische Laserscanner – Im Fokus der Genauigkeit. *Proceedings of 184th DVW-Seminar, Terrestrisches Laserscanning 2019*.

Lösler, M. (2024). *Java·Applied·Geodesy·3D (JAG3D) — Least-Squares Adjustment Software for Geodetic Sciences — software.applied-geodesy.org*. Applied-Geodesy.org. https://software.applied-geodesy.org/

Niemeier, W. (2008). *Ausgleichungsrechnung Statistische Auswertemethoden*. Walter De Gruyter.

Raschhofer, J., Kerekes, G., Harmening, C., Neuner, H., & Schwieger, V. (2021). Estimating Control Points for B-Spline Surfaces Using Fully Populated Synthetic Variance–Covariance Matrices for TLS Point Clouds. *Remote Sensing*, *13*(16).

Schmitz, B., Kuhlmann, H., & Holst, C. (2021). Towards the empirical determination of correlations in terrestrial laser scanner range observations and the comparison of the correlation structure of different scanners. *ISPRS Journal of Photogrammetry and Remote Sensing*, *182*.

Wieser, A., Pfaffenholz, J.-A., & Neumann, I. (2019). Sensoren, Features und Physik - Zum aktuellen Stand der Entwicklung bei Laserscannern. *Proceedings of 184th DVW-Seminar, Terrestrisches Laserscanning 2019*.

Yang, Y., Balangé, L., Gericke, O., Schmeer, D., Zhang, L., Sobek, W., & Schwieger, V. (2021). Monitoring of the production process of graded concrete component using terrestrial laser scanning. *Remote Sensing*, *13*(9)